2010 IEEE International Conference on Robotics and Automation
Anchorage Convention District
May 3-8, 2010, Anchorage, Alaska, USA

# Calibration of a Structure Light based Windshield Inspection System

Chi Zhang, Ning Xi, Jing Xu, and Quan Shi

*Abstract*— **Three dimensional optic measurement system's accuracy is highly related with the field of inspection. Increasing of field inspection costs increasing camera / projector pixel area on the test surface. Small surface changes within one pixel area cannot be directly detected, which will lower the system accuracy. A pixel-to-pixel strategy is developed to solve this problem. Increasing field of inspection also costs a longer standoff distance. The random image noise from the environment, uncertainties functions by lens distortion and resolution variation are all amplified. Therefore, a more complicated calibration model for each pixel is proposed to calibrate the system. In traditional structured light vision systems, a single sensor usually detects around 10,000 - 50,000 $mm^2$, and the 3D vision sensor in this paper needs to detect around 2,400,000 $mm^2$. Larger detection range gives more challenge to finish the calibration tasks. This paper proposes a clear calibration procedure to a large field of inspection structured light system. Last the comparison with the CMM measured results is used to prove that the calibration tasks have been successfully achieved.**

## I. INTRODUCTION

Development of rapid and accurate measurement systems for 3-D shape is an active research direction. Among the current existing 3D measurement techniques, structured light based 3D vision [1] has made giant strides in development and has been utilized in many applications [2] such as design, manufacturing, and inspection in recent decades. The necessary step to get an accurate 3D reconstruction by a structured light system is a proper calibration process. This paper focuses on the calibration of a given structured light system for a specific application.

Error analysis and calibration of a structured light system have been discussed for several decades in the past. Trobina [4] developed an error model for an active range sensor from the camera perspective geometry. Yang [5] proposed a more detailed mathematic model for several error sources and their effects in measuring 3D surface by structured light method. A relative error model [6] was presented for calibration of the active triangulation sensing model. Uncertainties analysis of the noise [7] [8] in vision systems has been discussed for their effects to the calibration performance. However, very few papers talked about the sensor consistence performance when random image noise was amplified by the large area of inspection.

3D point cloud generation can be viewed as finding the missing constraint in the camera projective transformation. In traditional methods, 3D point cloud is calculated by the intersections between the calibrated incident lights from the projector and the calibrated reflected lights to the camera. Both devices' calibrations are critical in data acquisition. Tsai [9] developed a detail calibration procedure for a camera with formulating several error models. Using a multi-plane method, Shi [10] formulated each implementation error source and calibrated a robot aided active vision system. Projectors are more difficult to calibrate compared with cameras, since they cannot receive any information. Recently, Mosnier [14] calibrated a projector by combination of pattern detection and visual servoing, Drareni [15] calibrated a projector with the aid from a calibrated camera. Zhang [11] proposed a self-calibration method using plane based homography with known intrinsic parameters of the camera and the projector.

Windshield Rapid Inspection System (WRIS) [12] is designed to be integrated into an industrial assembly line and examine each windshield pass by within 20 seconds, which requires the system robust and simple to operate. Structured light based active vision method is applied in such an application. Two challenges are met in designing WRIS:

1) A large inspection field is required due to the windshield size, which costs large pixel area on the tested surface and long standoff distance. Large pixel size requires a proper calibration of each pixel. Long standoff distance means both magnitude and the number of uncertainties are increased.

2) Projector's calibration error is usually bigger than camera's, since projection information cannot be directly acquired, which needs additional devices, additional calculations, and overall more complicated procedures. Projector's calibration error is further enlarged by the long standoff distance and large pixel area.

A new way to calculate the 3D point cloud is proposed in our paper, in which calibration of the projector is avoided by a different sensor model.

The camera first captures the projector's Gray Code and Line Shifting (GCLS) patterns on a flat surface, and then obtains the GCLS patterns again on a given surface. The deformation between two GCLS patterns is used to calculate a 2.5D height map. The height map is transformed to a 3D point cloud based on the projective geometry after camera calibration. Therefore, there is no need of projector calibration in the whole process. Since the principle model is different, existing calibration methods can not be applied to WRIS system.

A new calibration model based on pixel-to-pixel strategy is developed to calibrate the WRIS 3D sensor to conquer a large number of uncertainties. Statistical analysis of the random image noise has been simulated and compared with the

Chi Zhang, Ning Xi, Jing Xu are with Department of Electrical and Computer Engineering, Michigan State University, East Lansing, MI, 48824, USA zhangc11@msu.edu; xin@egr.msu.edu; xujing08@msu.edu

Quan Shi is with PPG Industries Inc., Glass Research Center, 400 Guys Run Road. Cheswick, PA, 15024, USA qshi@ppg.com

experimental results. Mean of multiple measurements is used to reduce the random noise in data collection. Homography matrix, representing the geometric relationship between two planes in 3D space, is calculated to cancel the resolution change due to the plane-to-plane-projection. Due to the large pixel size on the tested surface, each pixel is treated as individual calibration model. At last, a second order residual function is applied for each pixel to further improve the accuracy.

A clear calibration procedure of a structured light system is introduced in the following way: introduction and the calibration tasks for the 3D vision system are in section I; a clear calibration procedure for sensor calibration is explained in section II; section III solves the system calibration problem; section IV gives a comparison with CMM data; finally conclusions are given in section V.

### A. The 3 D vision system and the calibration tasks

WRIS is designed to scan a windshield, generate the outer surface point cloud and calculate the correspondent error distribution map with the design surface (CAD model). The configuration of the inspection system is shown in Fig. 1.

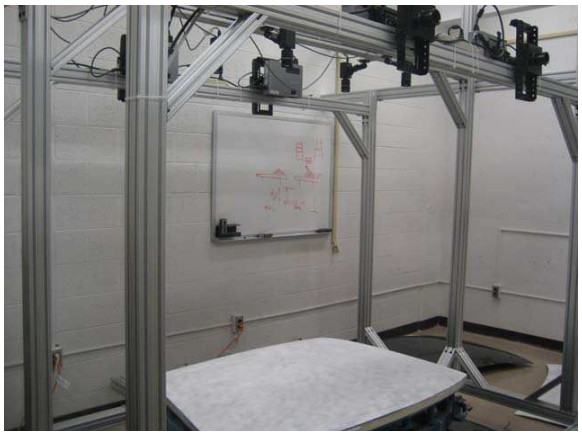

Fig. 1. WRIS system configuration.

The system is built at Michigan State University Robotics and Automation laboratory. Aluminum T slots are selected to build a frame structure. Four pairs of projectors and high resolution cameras (4 mega-pixels) are mounted on the upper beams to measure the windshield underneath. 3D point cloud is constructed by calculating the deformation of GCLS pattern by the tested windshield surface. Define the windshield surface in the world frame as

$$\mathrm{P^W} = \left\{ p_i^W \left(x_i, y_i, z_i\right) \in R^3 \right\} \tag{1}$$

and the point cloud in the sensor frame as

$$\mathrm{P^{S_j}} = \left\{ p_i^{S_j} \left(x_i, y_i, z_i\right) \in R^3 \right\}, j = 1,2,3,4 \tag{2}$$

The relation between point clouds in different sensor frames and the windshield surface in world frame can be denoted as

$$\mathrm{P^{S_j}} = T_W^{S_j} P^W, j = 1,2,3,4 \tag{3}$$

The registration of four point clouds into one entire one is denoted as:

$$P^C = \bigcup_{j=1}^{4} \left( T_{S_j}^C P^{S_j} \right), \tag{4}$$

in which, $P^C$ is the entire point cloud in the common frame.

Basically two tasks are required in this multi-sensor system calibration:

Sensor calibration: Evaluate the uncertainties and calculate all sensors parameters to acquire 3D point cloud without any deformation.

System calibration: Find the four Rigid registration transformation matrixes to common frame in this multi-sensor system.

The paper mainly focuses on the first one.

## II. THE CALIBRATION PROCEDURE.

The procedure for a general calibration task can be roughly separated into six steps: 1) working principle of the sensors, 2) system consistence tests, 3) error analysis, 4) establishment of a calibration model, 5) experiments and collection of data, and 6) parameters identification.

### A. The working principle of the sensors

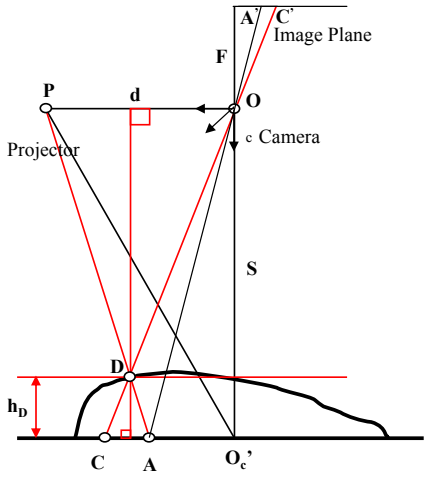


Fig. 2. The working principle of a WRIS sensor.

Fig. 2 shows the sensor working principle: $h_D$ represents the height from one surface point $D$ to the reference plane, $L_{AC}$ is the distance between points $A$ and $C$, $d$ is the baseline distance from points $P$ to $O$. Line $PO$ is assumed parallel with a reference plane, and $S$ is the standoff distance between line $PO$ and reference plane. Therefore, as long as $L_{AC}$, $d$, and $S$ are known, $h_D$ can be calculated using Eq. 5, which is derived according to similar triangle theory.

$$h_D = \frac{L_{AC} \bullet S}{d + L_{AC}} \tag{5}$$

### B. System consistence tests

System consistence performance is an old concept in robotics area, which evaluates the repeatability of a robot arm. However, in the machine vision area, few 3D vision calibration papers discussed it. This is because the random image noise is low in the traditional inspection range, 10,000 - 50,000 $mm^2$. Large range detection is only used for navigation purpose, which requires low accuracy.

Current system field of view is about 2,400,000 $mm^2$ with the inspection purpose. With almost 10 times large standoff distance, the random light intensity noise from the environment cannot be ignored anymore. The sub-pixel location for same surface point has a certain level variation.

*1) Consistence simulation:* From Eq. 5, once the input $L_{AC}$ has a certain magnitude of uncertainties, the height error will be:

$$h = \left| \frac{S}{1+\frac{d}{L_{AC}Res}} - \frac{S}{1+\frac{d}{(L_{AC}\pm L_{AC})Res}} \right|, \tag{6}$$

where *Res* represents the resolution converting the unit from *pixel* into *millimeter*. The system is assumed to have *0.1, 0.2, 0.3*, and *0.5* pixel error respectively, the errors in height are shown in the Fig. 3. *S* is approximately *1500 mm*. *d* is around *500 mm*, and *Res* equals *0.55 mm/pixel*, the average input of $L_{AC}$ is around 100 pixels in the real case.

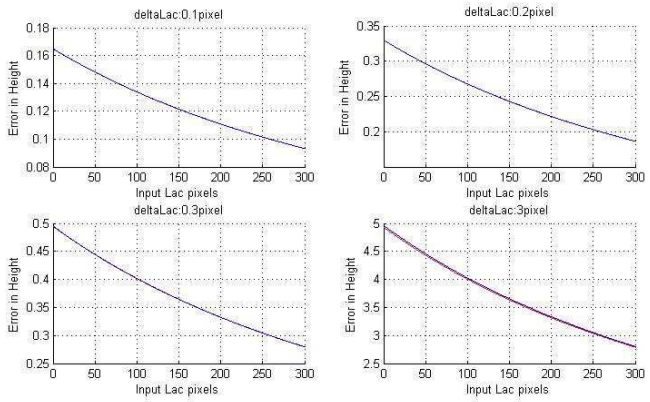


Fig. 3. Error analysis results, when the system has 0.1, 0.2, 0.3 and 0.5 pixels' error, the error amount in height.

*2) Consistence experimental results:* A given windshield is placed under the WRIS system and measured 10 times. The standard deviation is used to evaluate the consistence performance of the system.

From Eq. 5, every camera pixel's height map $h_n(i,j), n = 1,2,...,10$ is calculated, where $i$ and $j$ stand for the row and column location of a pixel.

The mean of the height map of each pixel is calculated by

$$\bar{h}_{(i,j)} = M(h_{(i,j)}) = \frac{1}{n}\sum_{k=1}^{k=n}(h_n(i,j)) \tag{7}$$

The standard deviation of each point is

$$Std_{(i,j)} = \sqrt{\frac{1}{n}\left(h_{(i,j)} - \bar{h}_{(i,j)}\right)^2} \tag{8}$$

TABLE I

THE STANDARD DEVIATION RESULTS FOR ALL SENSORS

| Sensor one | Sensor two | Sensor three | Sensor four |
|---|---|---|---|
| 0.17 mm | 0.08 mm | 0.08 mm | 0.13 mm |

The standard deviation of a point cloud can be calculated by

$$Std_s = \frac{1}{n_i \bullet n_j}(\sum_i \sum_j Std_{(i,j)}), (\mathrm{i} = 1..., \mathrm{n_i}, \mathrm{j} = 1, ...\mathrm{n_j}), \tag{9}$$

where $n_i$ and $n_j$ are the row and column numbers of the camera resolution, in this application they are *2002* and *2044*.

Consistence test results for all sensors are listed in Tab. I.

Comparing the simulation results with the experimental results in Tab. 1, there is around *0.1* pixel uncertainty noise in the input $L_{AC}$. The height map standard deviation is around *0.13 mm* in average.

### C. Error analysis

Random image noise from environment is amplified as the sensing system is designed bigger, and consistence of the system cannot be perfect. Implementation errors also make differences between the actual case and the theoretic model. Cameras and projectors cannot be perfectly perpendicular to the ground in practice, which costs the resolution change. Different pixels in $L_{AC}$ do not represent same length.

*1) Consistence error $E_{consistence}$:* Consistence analysis can be viewed as the starting point of the calibration job. Calibration results will never exceed the consistence performance. The mean of multi-measurements method is used to reduce this random error in data collection.

*2) Mis-alignment error from both a projector and a camera $E_{mis-align}$:* From the working principle of the system, each pixel's height map $h_{(i,j)}$ is calculated from input $L_{AC}(i,j) \bullet Res(i,j)$. If the flat reference plane is perfect parallel to the image plane, image pixel size on the reference will be constant. However, implementation always has a certain angle of mis-alignment.

In Fig. 4, the projector is designed to shoot a square image. Due to the mis-alignment error, the square pattern is changed by the homography matrix into a quadrangle. The shape will warp again when the camera captures the image of the pattern.

$$P_r = H_p^r I_P \tag{10}$$

$$I_C = H_r^C P_r, \tag{11}$$

in which, $I_P$ is the projector image coordinate, and $I_C$ is the camera image coordinate. $P_r = (x_r, y_r, 1)'$ is the world coordinate on the reference board, assuming $z = 0$ on the reference board. From Eq. 10 and Eq. 11, Homography matrix between camera image plane and projector image plane is shown as:

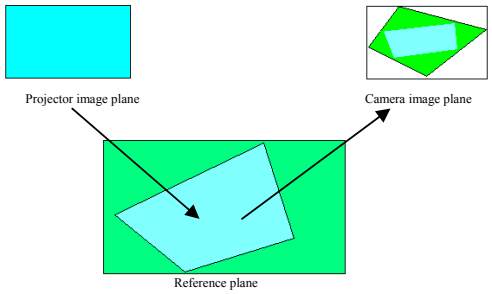


Fig. 4. 3-D case of the resolution difference.

$$I_C = H_r^C H_p^r I_P = H_P^C I_P \tag{12}$$

$$\begin{bmatrix} x_C \\ y_C \\ 1 \end{bmatrix} = \begin{bmatrix} h_{11} & h_{12} & h_{13} \\ h_{21} & h_{22} & h_{23} \\ h_{31} & h_{32} & h_{33} \end{bmatrix} \begin{bmatrix} x_P \\ y_P \\ 1 \end{bmatrix} \tag{13}$$

$L_{AC}$ in the sensor model can be transferred into projector plane in which the resolution keeps constant:

$$L_{AC}^C = Y_C^C - Y_A^C = H_P^C (Y_C^P - Y_A^P), \tag{14}$$

where, $L_{AC}^C$ is the pixel distance in camera frame, $Y_C^C$ and $Y_A^C$ are the pixel coordinates along $y$ direction in camera frame. $Y_C^P$, and $Y_A^P$ are the pixel coordinates along $y$ direction in projector frame.

Writing the $H$ matrix in vector form as $\vec{h} = (h_{11}, h_{12}, h_{13}, h_{21}, h_{22}, h_{23}, h_{31}, h_{32}, h_{33})^T$, and then the homogeneous equations for $n$ points become $Ah = 0$, with $A$ the $2n \times 9$ matrix:

$$A = \begin{pmatrix} x_1 & y_1 & 1 & 0 & 0 & 0 & -x_1X_1 & -y_1X_1 & -X_1 \\ 0 & 0 & 0 & x_1 & y_1 & 1 & -x_1Y_1 & -y_1Y & -Y_1 \\ x_2 & y_2 & 1 & 0 & 0 & 0 & -x_2X_2 & -y_2X_2 & -X_2 \\ 0 & 0 & 0 & x_2 & y_2 & 1 & -x_2Y_2 & -y_2Y_2 & -Y_2 \\ . & . & . & . & . & . & . & . & . \\ . & . & . & . & . & . & . & . & . \\ . & . & . & . & . & . & . & . & . \\ x_n & y_n & 1 & 0 & 0 & 0 & -x_nX_n & -y_nX_n & -X_n \\ 0 & 0 & 0 & x_n & y_n & 1 & -x_nY_n & -y_nY_n & -Y_n \end{pmatrix} \tag{15}$$

Vector $\vec{h}$ is solved by more four points in both image plane.

*3) Lens distortion error function $E_{dist}$:* The radius lens distortion model [9] is applied in the calibration model:

$$\begin{aligned} E_{dist} &= X_d - X_n = \left(1 + k_{c1}r^2 + k_{c2}r^4\right) X_n - X_n \\ &= \left(k_{c1}r^2 + k_{c2}r^4\right) X_n \end{aligned} \tag{16}$$

in which $X_n$ denotes the normalized coordinates $[x_n, y_n]'$, $X_d$ denotes the distorted one $[x_d, y_d]']$. $k_{c1}$ and $k_{c1}$ are the lens distortion coefficients.

### D. Calibration model

The error function $E$ contains several parts. Besides the consistence error, which is a random function, all the other parts need to be calibrated. Moreover, in order to reach pixel-to-pixel calibration accuracy, we can still improve each pixel's measurement accuracy by compensating each pixel's residual function. Given N layers on the coplanar calibration board, we can approximate the residual function by a non-linear second order function:

$$\begin{aligned} e_{i,(r,c)} &= H_{Measured,i} - H_{Idealmodel,i} \\ &= A_{(r,c)} \times L_{AC,i,(r,c)}^2 + B_{(r,c)} \times L_{AC,i,(r,c)} + C_{(r,c)}, \end{aligned} \tag{17}$$

where $H_{Measured,i}$ represents the true surface height in the $i^{th}$ measurement time. $H_{Idealmodel,i}$ is the output value of the theoretical calculation, and $e_{i,(r,c)}$ is the residual function which is approximated by a second order polynomial.

### E. Experiment procedure and collection of data

Vector $\vec{h}$ can be first calculated by shooting a grid pattern from the projector and receiving it by a camera. The corners coordinates of both images are found and used to calculate $\vec{h}$.

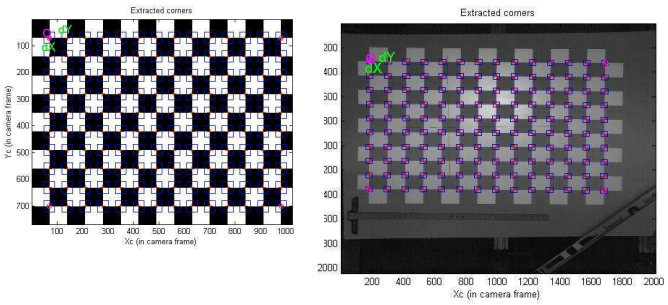


Fig. 5. (a) projector plane corner extraction, (b)camera plane corner extraction.

From the calibration model, the height information for each pixel needs to be examined multiple times. A multi-plane pixel-to-pixel calibration strategy has been developed. The calibration procedures which collect the reference data to estimate the system parameters are illustrated in Fig.6.

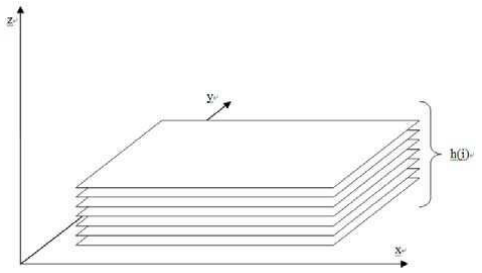


Fig. 6. Calibration strategy: Increasing the number of flat boards along its normal direction.

For each translation $n$ of the calibration board, the flat surface is measured five times. The input $L_{AC}$ for each pixel is denoted as $L_{AC,(r,c),i,n}, i = 1,2,..,5$.The mean of five measurements are calculated for each pixel so that the consistence error will reduce:

$$\bar{L}_{AC,(r,c),n} = \frac{1}{5}\sum_{i=1}^{5} \bar{L}_{AC,(r,c),i,n} \tag{18}$$

The mean of each pixel's height over the whole image plane will be used in the calibration model:

$$\bar{L}_{AC,n} = \frac{1}{N}\sum_{r=1}^{2008}\sum_{c=1}^{2004} L_{AC,(r,c),n}, \tag{19}$$

where $N$ is the number of measured pixel in the camera image. The results and distributions of $L_{AC}$ for each layer are shown in Fig. 7. Each layer's $L_{AC}$ can be viewed as a Gauss distribution due to the several implementation errors. The mean of each layer's $L_{AC}$ is applied to the sensor model to calculate $S$ and $d$.

From the calibration model, the first step is to find $S$ and $d$ by Eq. 15.

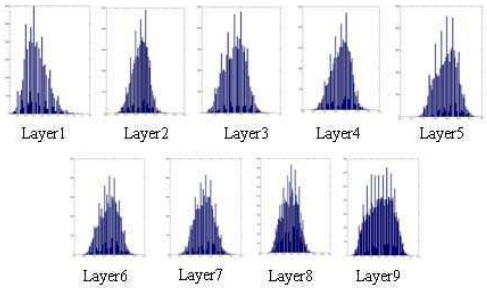


Fig. 7. Each layers' $L_{AC}$ distribution.

$$H_{true,n} \approx H_{system,n} = \frac{S}{(d/\bar{L}_{AC,n})+1}, n = 1,2,...,9 \tag{20}$$

$$\begin{bmatrix} H_1 & -\bar{L}_{AC,1} \\ ... & ... \\ H_n & -\bar{L}_{AC,n} \end{bmatrix} \begin{bmatrix} d \\ S \end{bmatrix} = \begin{bmatrix} -H_1\bar{L}_{AC,1} \\ ... \\ -H_n\bar{L}_{AC,n} \end{bmatrix}, n = 9 \tag{21}$$

By substituting the $\bar{L}AC,n$ and $H_{true,n}$ into Eq. 21, $S$ and $d$ are calculated by least square method. The coefficients $A_{(r,c)}$, $B_{(r,c)}$ and $C_{(r,c)}$ in the residual function for each pixel are calculated by the subtraction between $H_{true,n}$ and $H_{system,n}$.

$$\begin{aligned} e_{(r,c),n} &= H_{true,n} - \frac{S}{(d/L_{AC,(r,c),n})+1} = \\ & A_{(r,c)} \bullet L^2_{AC,(r,c),n} + B_{(r,c)} \bullet L_{AC,(r,c),n} + C_{(r,c)} \end{aligned} \tag{22}$$

### *F. Experimental results and parameters identification*

Following the calibration model in step $D$ and the collected data in step $E$, sensor calibration parameters are estimated in Table 2. The first line is the ground true height for each layer. The sensor's output values are shown in the second line. The differences between these two are listed in the third line. All units are in mm.

## III. SYSTEM CALIBRATION

Four rigid registration matrixes are needed to transfer 4 individual point clouds into a common frame.

TABLE II

CALIBRATION RESULTS BASED ON $\bar{L}_{AC,n}$.

| | | | | | | | | |
|---|---|---|---|---|---|---|---|---|
| Sensor 1: S = 1577.66 d = 451 | | | | | | | | |
| 19. 56050. | 39. 42080. | 43. 05550. | 46. 81220. | 50. 55870. | 54. 56430. | 58. 45810. | 62. 23250. | 81. 88960. |
| 19. 711414. | 39. 411938. | 43. 348502. | 47. 36072. | 50. 8494. | 54. 6438. | 58. 25887. | 62. 14839. | 81. 58578. |
| 0. 150914. | −0. 00886. | 0. 293002. | 0. 54852. | 0. 29079. | 0. 07954. | −0. 19922. | −0. 08410. | −0. 30381. |
| Sensor 2 : S = 1584.20 d = 459. | | | | | | | | |
| 19. 56050. | 39. 42080. | 43. 05550. | 46. 81220. | 50. 55870. | 54. 56430. | 58. 458100. | 62. 23250. | 81. 88960. |
| 19. 75963. | 39. 19303. | 42. 84934. | 46. 47487. | 50. 9659. | 54. 80492. | 58. 461467. | 62. 38606. | 81. 42030. |
| 0. 199130. | −0. 22777. | −0. 20615. | −0. 33733. | 0. 407198. | 0. 240618. | 0. 003367. | 0. 15356. | −0. 46930. |
| Sensor 3 : S = 1568.32 d= 429. | | | | | | | | |
| 19. 56050. | 39. 42080. | 43. 05550. | 46. 81220. | 50. 55870. | 54. 56430. | 58. 45810. | 62. 23250. | 81. 889600. |
| 19. 92812. | 38. 90314. | 42. 56365. | 46. 61080. | 50. 62836. | 54. 65578. | 58. 46443. | 62. 32670. | 81. 489819. |
| 0. 367615. | −0. 51766. | −0. 49185. | −0. 20139. | 0. 069662. | 0. 091487. | 0. 006331. | 0. 094206. | −0. 399781. |
| Sensor 4: 1569.27 431. | | | | | | | | |
| 20. 56050. | 39. 42080. | 43. 05550. | 46. 81220. | 50. 55870. | 54. 564300. | 58. 458100. | 62. 232500. | 80. 889600. |
| 21. 24124. | 39. 93037. | 43. 76641. | 47. 39353. | 50. 86657. | 54. 560074. | 58. 406414. | 61. 918873. | 80. 639268. |
| 0. 680747. | 0. 509577. | 0. 710913. | 0. 581332. | 0. 307870. | −0. 004226. | −0. 051686. | −0. 313627. | −0. 250332. |

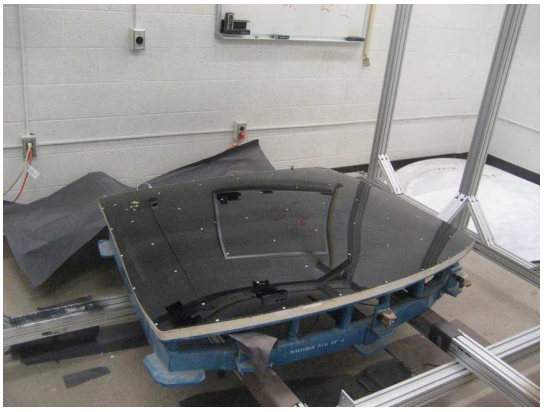

Fig. 8. The system calibration gage.

In Fig. 8, white dot marker's center coordinates are measured by CMM. The rest of the part has been painted into black so that only white dots are measured. From Eq. 3, the transformation $T$ is calculated between two measurement results after correspondence is found by a modified ICP method [13]. Fig. 9 shows the system calibration results, four small pieces of point clouds join into one.

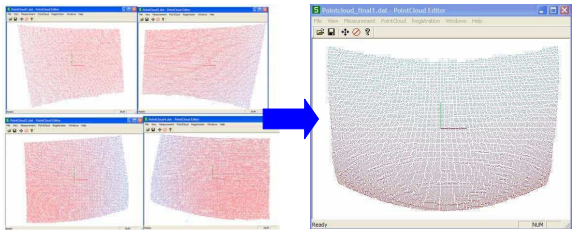

Fig. 9. (a) Four point clouds. (b) The final point cloud.

## IV. CALIBRATION RESULTS AND EVALUATION

After the system has been calibrated, a new piece of windshield which has been pre-measured by a CMM is used to evaluate the system overall performance. Both systems' measurement results: measured point clouds and error maps, are put together to compare with each other. Since CMM has been used in industry for years, its data can be considered as a standard. The consistence with CMM data will demonstrate the success of WRIS calibration.

The CMM measurement point cloud is denoted as $\{P_{CMM}(x_i^C, y_i^C, z_i^C) \in R^3\}$ , and the WRIS result is denoted as $\{P_{WRIS}(x_i^W, y_i^W, z_i^W) \in R^3\}$ , The mean error is used to find the difference between both point clouds:

$$Mean = \frac{1}{N}\sum_{i=1}^{N}\left[(x_i^W - x_i^C)^2 + (y_i^W - y_i^C)^2 + (z_i^W - z_i^C)^2\right]^{1/2} \quad (23)$$

The difference between CMM data and WRIS data is about 0.15 mm, which is around 0.14 pixel in backprojected images into cameras. Compared with the results [11], their overall backprojected pixel errors are 0.02 pixel in camera and 0.29 pixel in projector. Since in our sensor model the projector's intrinsic and extrinsic parameters do not participate in the calculation, 3D points in world are directly correspondence with projector pixels. Backprojected error in projector can be viewed as 0 pixel.

Fig. 10 and Fig. 11 illustrate that both CMM data and the WRIS point cloud has the similar error distribution shape and the same error color magnitudes.

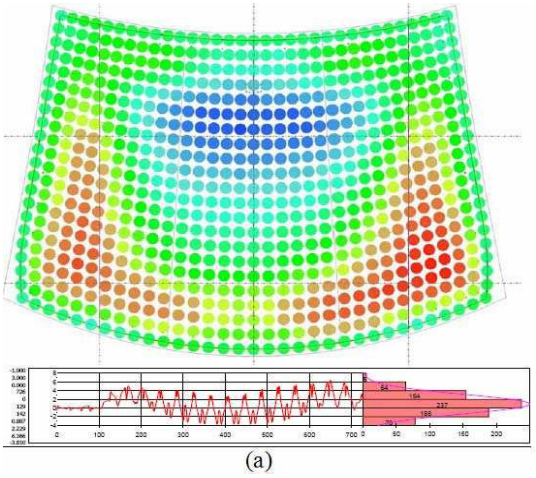


Fig. 10. The CMM error map.

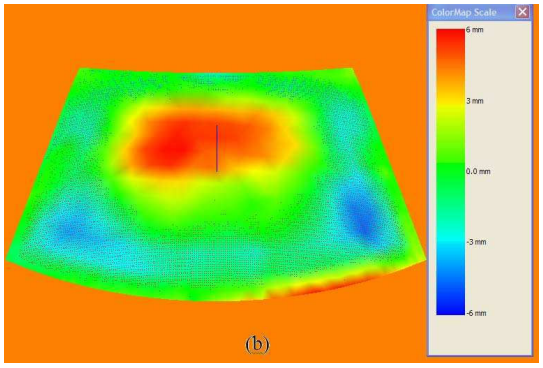


Fig. 11. The WRIS error map.

## V. CONCLUSION

A clear calibration procedure of a structure light vision system has been implemented when the 3D sensor has a relatively large field of inspection. Calibration tasks can be separated into two categories: sensor calibration and system calibration. The main effort is concentrated on the sensor calibration. A detailed calibration model and error analysis are developed due to the increasing number of uncertainties. Pixel-to-pixel calibration strategy is applied to reach the accuracy requirement. System calibration uses Iterative Closed Point (ICP) [13] method to solve the correspondence problem and calculates the rigid transformation matrix between each sensor to world frame. The calibrated WRIS is able to sample a given piece of windshield and generate a point cloud of more than 30000 points within 20 seconds. Experimental results show the system calibration results are comparable with a CMM system. The calibration method is feasible for the task.

## REFERENCES


[1] Pages J, Salvi J, Garcia R, and Matabosch C. Overview of coded light projection techniques for qutomatics 3 D profiling, *In Proceedings of IEEE international conference on robotics and automation*, Taipei, Taiwan, 2003, pp. 133-138.

[2] Kurada, S., and Bradley. C., A review of machine vision sensors for tool condition monitoring, *Comput. Ind.*, 34, No. 1, pp. 55-72, 1997.

[3] Q. Shi, N. Xi, and H. Chen, "Integrated process for measurement of free-form automotive part surface using a digital area sensor," in IEEE International Conference on Robotics and Automation,Alera, Canada, 2005, pp.1526- 1531.

[4] M. Trobina, "Error Model of a Coded-Light Range Sensor," BIWI-TR-164, Sept. 21, 1995.

[5] Z. Yang, and Y.F. Wang, Error Analysis of 3 D Shape Construction from Structured Lighting, *Pattern Recognition*, Vol. 29, No. 2, pp. 189-206, 1996.

[6] G. Sansoni, M. Carocci, and T. Rodella, Calibration and Performance Evaluation of a 3-D Imaging Sensor Based on the Projection of Structured Light, *IEEE Transactions on Instrumentation and Measurement*, Vol. 49, No. 3, pp. 628-536, 2000.

[7] P. Chen and D. Suter, "Homography estimation and heteroscedastic noise-a first order perturbation analysis," Monash University, Tec. Rep. MECSE-32, 2005.

[8] R. Hartley and A. Zisserman, Multiple View Geometry in Computer Vision, Cambridge U.Press, 2003, Chap. 5, pp.132 - 150.

[9] R. Tsai, A Versatile Camera Calibration Technique for High-Accuracy 3D Machine Vision Metrology Using Off-the-Shelf TV Cameras and Lenses, *IEEE Journal of Robotics and Automation*, Vol. Ra-3, No. 4, 1987.

[10] Q. Shi, N. Xi, H. Chen, and Y. Chen, "Calibration of Robotic Area Sensing System for Dimensional Measurement of Automotive Part Surfaces," in International Conference on Intelligent Robots and Systems, Alberta, Canada, Aug. 2005, pp. 1526-1531.

[11] B. Zhang, and Y. Li, Dynamic calibration of the relative pose and error analysis in a structured light system, *J. Opt. Soc.*, Vol. 25, No. 3.pp 612 -622. March. 2008.

[12] C. Zhang, N. Xi, Q. Shi, "Object-Orientated Registration Method for Surface Inspection of Automotive Windshields," *in International Conference on Intelligent Robots and Systems*, Nice, France, Sep. 2008, pp. 3553-3558.

[13] P. J. Besl and N. D. Mckay, A Method for Registration of 3-D Shapes, *IEEE Transactions on Pattern Analysis and Machine Intelligence*, vol. 14. no.2, 1992, pp 239-255.

[14] J. Mosnier, F. Berry and O. A. Aider, "A New Method for Projector Calibration Based on Visual Servoing," *in IAPR Conference on Machine Vision Applications*, Yokohama, Japan, May 20-22, 2009, pp 25-29.

[15] J. Drarei, and S. Roy, "Projector Calibration Using a Markerless Plane," *in Proceedings of the Interenational Conference on Computer Vision Theory and Applications*, Lisbon, Portugal, Feb 2009, volume 2, pp 377 -382.